# Palaeostress and geotectonic interpretation of the Alpine Cycle onset in the Sierra del Guadarrama (eastern Iberian Central System), based on evidence from episyenites

J.M. González-Casado [a,*], J.M. Caballero [b], C. Casquet [b], C. Galindo [b], F. Tornos [c]

[a] *Departamento de Q.A., Geología y Geoquímica. Universidad Autónoma de Madrid, 28049-Madrid. Spain*
[b] *Departamento de Petrología y Geoquímica, Universidad Complutense de Madrid, 28040-Madrid, Spain*
[c] *Instituto Tecnológico y Geominero, 28003-Madrid, Spain*

**Abstract**

Several episodes of hydrothermal activity related to periods of fracturing and/or reactivation of previous structures took place from 300 to – at least – 100 Ma, in the Sierra del Guadarrama, which is part of the crystalline axis of the Iberian Hercynian Fold Belt (Central-Iberian Zone). One of these episodes led to the formation of episyenites, which are de-quartzified and alkalinized granites. Episyenite formation took place on a regional scale and in a short period (approx. at 277 Ma). The episyenites were formed by the action of fluids at temperatures between 350°C and 650°C, at depths of about 6.5 km, and in microfractured dilatancy zones developed under a regional extensional regime. These zones are crosscut by normal faults, developed during the progressive deformation process accompanying the formation of the episyenites.

The calculated regional palaeostress tensor has $\sigma_1$ close to vertical and $\sigma_3$ between N10-20E and an average value of the stress ratio ($\Phi$) of 0.19 [$\Phi = (\sigma_2 - \sigma_3)/(\sigma_1 - \sigma_3)$]. Because $\sigma_1$ is close to vertical the stress tensor is compatible with an extensional deformation field. The analysis also shows that most of the faults that slip under this stress field have an average coefficient of friction of 0.8.

This extensional regime was probably accompanied by a regional thermal anomaly, as suggested by the high temperature of the fluids involved, which are amagmatic. This thermo-tectonic episode is interpreted as representative of the generalized extensional regime corresponding to the onset of the Alpine Cycle. The episode was preceded by a wrench-faulting event, equivalent to the Late Variscan event of Arthaud and Matte (1977), for which an age of – at least – 300–290 Ma is indicated by recent radiometric data. In its turn, this event was preceded by the regional extensional gravitative collapse of the Hercynian orogen. A correlation between evidence from the cover (stratigraphy and volcanism) and evidence from the basement (hydrothermal alterations, dyke injection episodes and granitic magmatism) is attempted on the basis of new available radiometric data.

## 1. Introduction

One point of controversy in the geology of the Iberian Hercynian realm is the tectonic history from the end of the Hercynian orogeny to the beginning of

* Corresponding author. FAX 34-1-3974900. e-mail Casado@ccuam3.sdi.uam.es.

the rifting that led to the opening of the Neo-Thethys alpine sedimentary basins, i.e., the onset of the Alpine cycle in southern Europe (Salas and Casas, 1993). The period of interest covers the time from the Late Carboniferous to the beginning of the recorded Mesozoic sedimentation, i.e., Early Triassic. This controversy is particularly intense in central Spain, where a complex interplay of faulting, sedimentation, volcanism, dyke injection and hydrothermal activity is well displayed (e.g., Arthaud and Matte, 1977; Vegas and Banda, 1982; Capote et al., 1987; Sopeña et al., 1988; Casquet et al., 1988; González-Casado et al., 1993; Doblas et al., 1994).

To a large extent, the problem arises from the lack of precise dating. Only recently have absolute dating of the dyke swarms (Galindo et al., 1994b) and of the hydrothermal alterations found in the basement (Caballero et al., 1992) become available. These data, along with a revision of former ages of granitoids and volcanics in the area, provide new constraints to the controversy. Particularly useful in this respect is the combined dating of hydrothermal alteration accompanied by fault analysis of the correlated fracturing, since it allows ages to be assigned to definite tectonic events, which, in turn, can be interpreted in terms of a regional geodynamic setting. The purpose of this work is twofold: (a) To accurately determine the palaeostress tensor (orientation and stress ratio, $\Phi$) for a set of faults associated with a particular type of hydrothermal alteration of Permian age, i.e., episyenitization, that is developed on a regional scale in the crystalline basement. Precise dating of episyenites is now available, as well as a good knowledge of their petrology including depth, $P_{fluid}$ and temperature of formation (Caballero, 1993). The depth–$P_{fluid}$–$T$ values permit estimation of the magnitude of the stress tensor. (b) To fit the inferred palaeostress tensor, along with other geological evidence, within an appropriate tectonic framework for the Late Carboniferous–Early Triassic period in central Spain.

## 2. Geological setting

The Sierra del Guadarrama is a crystalline intraplate mountain range situated in the central part of the Iberian Peninsula. It is a segment of the Iberian Central System (ICS), which trends ENE–WSW from central Spain into Portugal, separating the Duero and Tajo Cenozoic sedimentary basins (Fig. 1). The ICS was largely built up in the Miocene, during a contractional tectonic event that uplifted blocks of the Hercynian basement. It ends abruptly against the Iberian Range, to the east, which is another NW–SE-trending intraplate alpine chain, composed of Permian to Tertiary folded sediments.

The Sierra del Guadarrama consists largely of rocks belonging to the Hercynian basement and of a locally preserved thin cover of Upper Cretaceous sedimentary rocks. The basement rocks forming the Sierra del Guadarrama are composed of granitoids and high- to medium-grade metamorphic rocks, mostly Early Ordovician orthogneisses (Vialette et al., 1987; Gebauer et al., 1993), and some older metasediments. Towards the Iberian Range, scattered relics of small Permian detrital basins, and of a Triassic and Jurassic cover, are also preserved. These sedimentary rocks probably once existed in the Sierra del Guadarrama realm, but were eroded during the Early–Middle Cretaceous. A set of ENE–WSW-trending, high-angle reverse faults divides the Sierra del Guadarrama into several longitudinal blocks, with a pop-up geometry. The boundaries of the basement with the Tajo and Duero basins are two high-angle reverse faults with a large vertical displacement (> 1500 m). Most of these faults are interpreted as Late-Hercynian structures that were subsequently reactivated several times up to the present. The transit to the Iberian Range is marked by several NW–SE-trending strike-slip faults, which acted as transfers to the thrusts during Miocene contraction. Restored cross-sections through this part of the ICS suggest that the basement blocks were uplifted and slightly tilted by Miocene tectonics (De Vicente et al., 1992, 1996).

Granitoids are of particular interest, as they are the sites of most of the hydrothermal alteration dealt with here. These granitoids form the Guadarrama Batholith, and were emplaced in the time range 345–285 Ma (Vialette et al., 1981; Ibarrola et al., 1987; Pérez-Soba, 1991; Casillas et al., 1991; Caballero, 1993). This plutonism followed the main Hercynian orogenic phases, and consisted primarily of peraluminous monzogranites to leucogranites, with minor rocks of more basic composition. A remark-

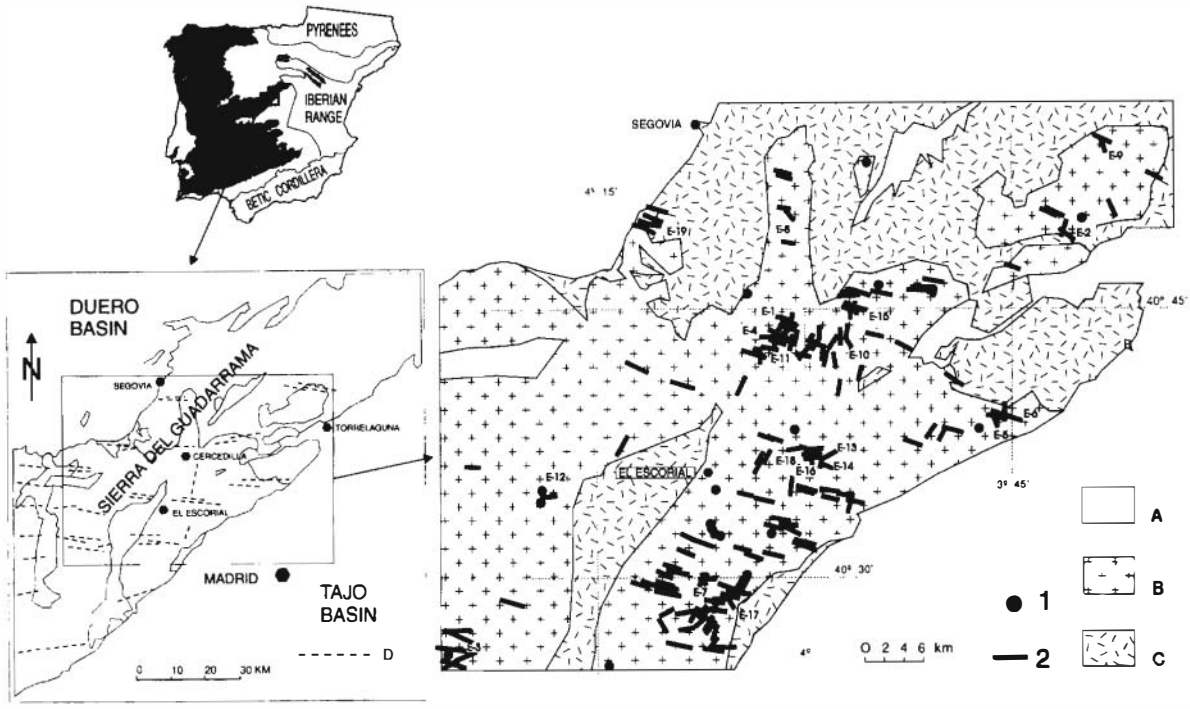


Fig. 1. Geological sketch of the Sierra del Guadarrama, showing the location of episyenitic bodies. *A* = post-Hercynian sediments; *B* = Hercynian granites; *C* = metamorphic rocks. Bars (*2*) represent surface-projected trends of episyenites; dots (*1*) are bodies with an unknown trend. The inset shows the location of the studied area within the Iberian Central System (ICS). *D* = main granitoid porphyries dyke swarms.

able feature of the Sierra del Guadarrama is the occurrence of long (up to 50 km), roughly parallel dyke swarms consisting of granitoid porphyries and of minor microdiorites. The trend of these dykes varies from N-90 to 120-E, though odd directions are locally recorded. One E–W-trending granitic dyke has been dated at 296 ± 3 Ma (Rb/Sr whole rock, Galindo et al., 1994b). Some N–S-trending dykes, only exposed in the central part of the Sierra del Guadarrama, define a younger orthogonal swarm, similar in composition to the first. A younger set of a few dykes of alkaline affinity, i.e., monzonitic (Huertas, 1991), is also present, and has been dated at 245 ± 7 Ma (Galindo et al., 1994b).

The Sierra del Guadarrama hosts many types of alterations corresponding to fracture-controlled episodes of hydrothermal activity. These include: (1) 300–290 Ma W–(Sn–Mo) lodes and Sn–(W) greisens, related to a strike-slip event. This episode is very close in time to the emplacement of the porphyry dykes; (2) 277 Ma episyenites (Fig. 1); (3) 151–156 Ma, quartz–chlorite–sericite replacements and Ba–F (Pb–Zn) lodes; and (4) 100 Ma quartz lodes related to another strike-slip episode (Tornos, 1989; Caballero et al., 1992; Caballero, 1993; González-Casado et al., 1993; Tornos et al., 1993; Galindo et al., 1994). Because of its Permian age, the alteration of the episyenitic type is particularly useful in constraining the history of the Hercynian–Alpine Cycle transition.

## 3. Episyenites

### *3.1. Petrological and chronological features*

Episyenites are rocks that originate from the dissolution of quartz from a granite, accompanied by alkali metasomatism (either Na or K), by the interaction with hydrothermal fluids (Leroy, 1982; Cathelineau, 1985). In the Sierra del Guadarrama, the episyenites replace either gneisses, dykes or grani-

toids, though the latter are by far the main host of this type of alteration. The episyenites are of the albitic type, and three varieties have been distinguished: pyroxenic, amphibolic and biotitic, according to the dominant mafic mineral. The formation temperature ranges from approximately 650°C (pyroxene-types) to 350°C (biotite-types). Nevertheless, most episyenitic samples (approx. 90%) are albite–chlorite types – and to a lesser extent microclinites – formed by low-temperature (< 350°C) alteration of the previous types (Caballero et al., 1991 and Caballero, 1993).

Episyenites were formed through the pervasive interaction with amagmatic aqueous fluids of low to moderate salinity (< 12 wt.% NaCl equiv.), along fracture bands. Fluid pressure and temperature during formation of the episyenites have been estimated by combining primary fluid inclusions, microthermometric data in mafic minerals and stable isotope thermometry (Caballero, 1993). Corrected fluid pressures are in the range 150 to 170 MPa, and represent trapping conditions once the hydrothermal system has become almost sealed. This is because mafic minerals are texturally late with respect to the main albitic alteration and leaching of quartz (Fig. 3C,D). Consequently, these pressures are probably close to lithostatic pressures. In this region, with an average density of granites of 2.6 to 2.65 $Mg/m^3$, the highest pressure recorded (170 MPa) corresponds to a depth of 6.5 km, which must be taken as a minimum depth for episyenite formation. This depth value will be used in subsequent computations in this work. Moreover, when quartz dissolution and replacement of igneous feldspars by albite took place, fluids had to be under an approximately hydrostatic pressure, as suggested by $P$–$T$ solubility data for quartz: retrograde solubility of quartz is only possible at $P_{fluid} \leq$ 100–110 MPa, under fluid salinities equivalent to those found here (Casquet et al., 1992; Zhixin and Walther, 1993). Thus, the whole process of episyenite formation probably took place under a cyclic pressure regime.

The distribution of alteration is regional, suggesting that the episyenites are younger than metamorphism and subsequent magmatism. The age of the alteration is known through several Rb–Sr internal isochrons and K–Ar determinations, the latter carried out on biotites and amphiboles belonging to slightly to completely retrograde varieties. The samples were collected from both NNE–SSW- and E–W-trending episyenitic bodies. Two Rb–Sr isochron ages (278 ± 3 and 274 ± 4 Ma) and two regression ages (279 ± 34 and 276 ± 9 Ma), (Casquet et al., 1992; Caballero, 1993), suggest that the formation of episyenites was an almost isochronous process in the whole Sierra del Guadarrama, and took place in the Early–Permian. The K–Ar apparent ages vary from 266 to 216 Ma. A correlation with the degree of low temperature alteration of the episyenites (chlorite formation and replacements by K-feldspar, i.e., microclinites) is envisaged, suggesting that retrogression took place during (at least) one superimposed alteration event (Caballero et al., 1992, 1993; Caballero, 1993). In this respect it is noteworthy that there is a coincidence of most K–Ar ages (216–235 Ma) with intrusion of monzonitic dykes (220–245 Ma).

### *3.2. Structural features of the episyenitic bodies*

Most episyenites are subvertical (> 85°) lens-shaped bodies arranged as swarms, with trends close to N-110-E (57% of the bodies) and NNE–SSW (30%) (Figs. 1 and 2A). Low dips (those as low as 70°) are very rarely found and are probably related to younger local block tilting. The vertical extensions of these bodies can be several tens of meters, disappearing abruptly at depth. Thicknesses range from a few centimeters to tens of meters, and length varies from 3 to 300 m. The swarms sometimes extend for a considerable distance, e.g., 2 to 3 km. Contacts of episyenites with the host rocks are sharp (Fig. 3A), and offsetting is not observed when they crosscut passive markers, such as aplite dykes or granite contacts.

A pervasive cataclastic fabric, restricted to the episyenitic band, was developed coevally with the hydrothermal process (Caballero, 1993)(Fig. 3B). Feldspars display recrystallization to a variable extent (mantle–core textures, with the core showing internal deformation) (Fig. 3C,D), while the mafic minerals often display cataclastic granulation accompanied by replacement by other mafic minerals (Fig. 3C). The deformation inside the episyenitic body is also accommodated by minor tension gashes (filled with mafic minerals) and faults. The fault density is

variable from one place to another, and many episyenites do not show any faulting at all, while others present abundant fault planes largely restricted to the interior or close to the altered body. Furthermore, no relationship seems to exist between the distribution of the episyenites and major regional faults.

The pervasive cataclastic fabric itself is indicative of dilatancy (Rutter, 1986). Moreover, the very high fluid/rock ratios inferred from stable isotopes and REE-based mass balance considerations (Caballero, 1993) suggest that the permeability was high. Thus, stress-induced permeability remains the most reasonable mechanism to enhance fluid flow, percolation of the hydrothermal fluid taking place along an anastomosing network of microfractures developed in discrete dilatancy zones. The fact that episyenitic bodies are not shear bands, and that they cannot be related to major fractures, strongly suggests that these dilatancy zones must be interpreted as prefailure damaged regions, where minor faults eventually nucleate. The arrangement of the episyenitic bodies as swarms, the similar age and the regular trends they show on a regional scale suggest that a regional stress field was involved in the generation of the dilatancy zones. Local inhomogeneities probably controlled the site of nucleation of the bodies.

Experimental studies demonstrate that irreversible dilatancy, prior to faulting, occurs mainly through the development of tensional microcracks – even in

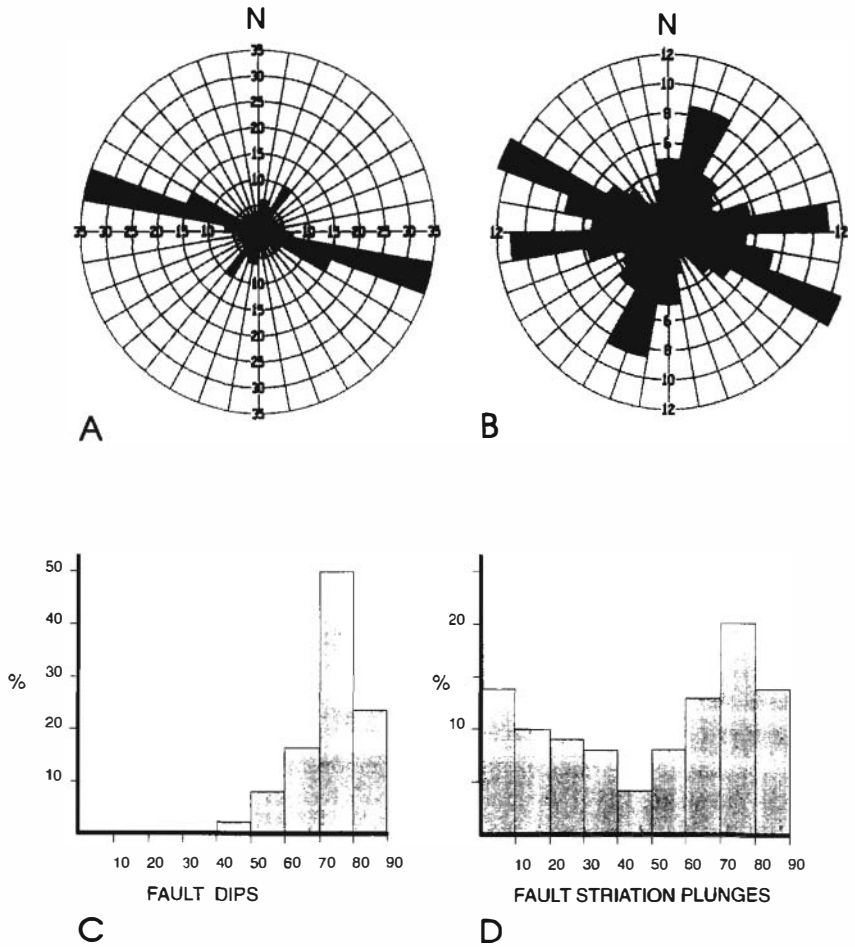


Fig. 2. Rose diagrams corresponding to: (A) distribution of surface-projected trends of the episyenitic bodies; (B) trends of faults related to episyenites; (C) histograms of fault dips; and (D) fault striation plunges.

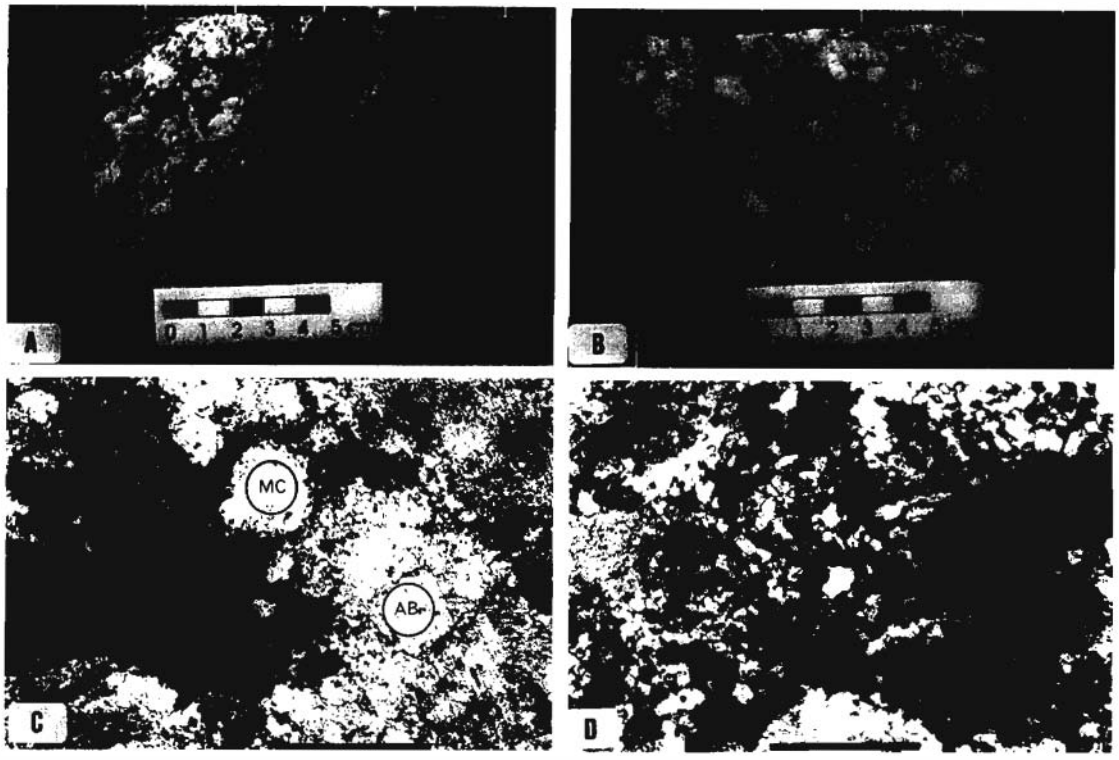


Fig. 3. Examples of deformational fabrics in episyenites. (A) Sharp episyenite(right)–granite(left) contact. Absence of quartz in the episyenite is noteworthy. (B) Episyenite with a macroscopic cataclastic fabric. (C) Albite and microcline crystals showing core–mantle textures. During an earlier stage of the episyenitic process granitic quartz was leached and igneous feldspar albitized. Microcline here is a relic igneous mineral. During subsequent stages (within the same alteration process), core–mantle textures developed along with the formation of mafic minerals (in this case biotite and amphibole). Scale bar 1 mm. Crossed polars. (D) Detail of a core–mantle texture developed in albite, wich itself resulted from the replacement of igneous feldspar. Scale bar 0.25 mm. Crossed polars.

a compressional environment – and that these microcracks are arranged parallel to the maximum principal stress axis (Holcomb and Stevens, 1980; Atkinson, 1984). However, there is little experimental evidence as to the orientation of the prefailure dilatant volume, though some experimental studies, in which heterogeneous dilatancy took place, strongly suggest that the orientation of the dilatant volume must also be parallel to the maximum principal stress (Yanagidani et al., 1985; Yukutake, 1989). Fractures, eventually nucleating inside the damaged volume, propagate outwards, towards the undilatant volume, with an oblique orientation respective to the maximum loading ($\sigma_1$) and dilatant region, as is expected from failure criteria (Yukutake, 1989, fig. 16; Lockner et al., 1991).

Extensive-dilatancy anisotropy, i.e., development of microcracks perpendicular to the minimum principal compressional stress, is well known in nature (Crampin, 1987; Lovell et al., 1990). With respect to the orientation of prefailure dilatant volumes, the best geological evidence comes from the works of Lespinasse (1984) and Pecher et al. (1985) on some episyenites from the French Central Massif. They demonstrate that the development of dilatancy zones is heterogeneous, episyenites forming at the regions of maximum dilatancy, and that a parallelism exists between the planes defined by the episyenitic bodies and populations of microcracks (fluid inclusion planes) developed in the neighbouring non-altered rocks. In other words, episyenites form normal to the direction of the minimum principal stress axis.

## 4. Determination of the stress regime during episyenite formation

### *4.1. Analytical procedure*

In recent years, several methods have been proposed to determine stress orientation and stress ratio using fault slip data (e.g., Carey and Brunier, 1974; Angelier, 1979, 1989; Etchecopar et al., 1981; Michael, 1984; Simón Gómez, 1986; Reches, 1987; Etchecopar and Mattauer, 1988). The procedure and the methods employed here are outlined below:

– First, with all the faults measured at each location, an average orientation of the principal stresses, $\sigma_1$ and $\sigma_3$, is calculated, using the right dihedra method (Angelier and Mechler, 1977). This method relies on the assumption that all the faults slip together under a single and uniform stress tensor. In consequence, it is be possible to define areas of compression (P) and tension (T) common to all faults in the set. The principal stresses $\sigma_1$ and $\sigma_3$ are located inside these areas. No information about the stress ratio can be obtained. Also, this procedure does not allow us to distinguish between faults formed during the episyenitic episode and others. However, the position, dispersion, cluster and angular relationships with and between the P and T regions allow to infer whether more than one fault set is present or not (Lisle, 1987; Casas Sainz et al., 1988; De Vicente et al., 1992b).

– Second, the stress inversion method proposed by Reches, (Reches, 1987 and Reches et al., 1992) was used. This method provides a mean stress tensor that fits the slip of a set of measured faults and striae with a minimum misfit. Like other methods (e.g., Angelier, 1979; Etchecopar et al., 1981; Michael, 1984), it relies on the Wallace–Bott relationship, i.e., the slip along a fault takes place in the direction of the maximum resolved shear stress (Wallace, 1951; Bott, 1959). Moreover, this method assumes that: (1)

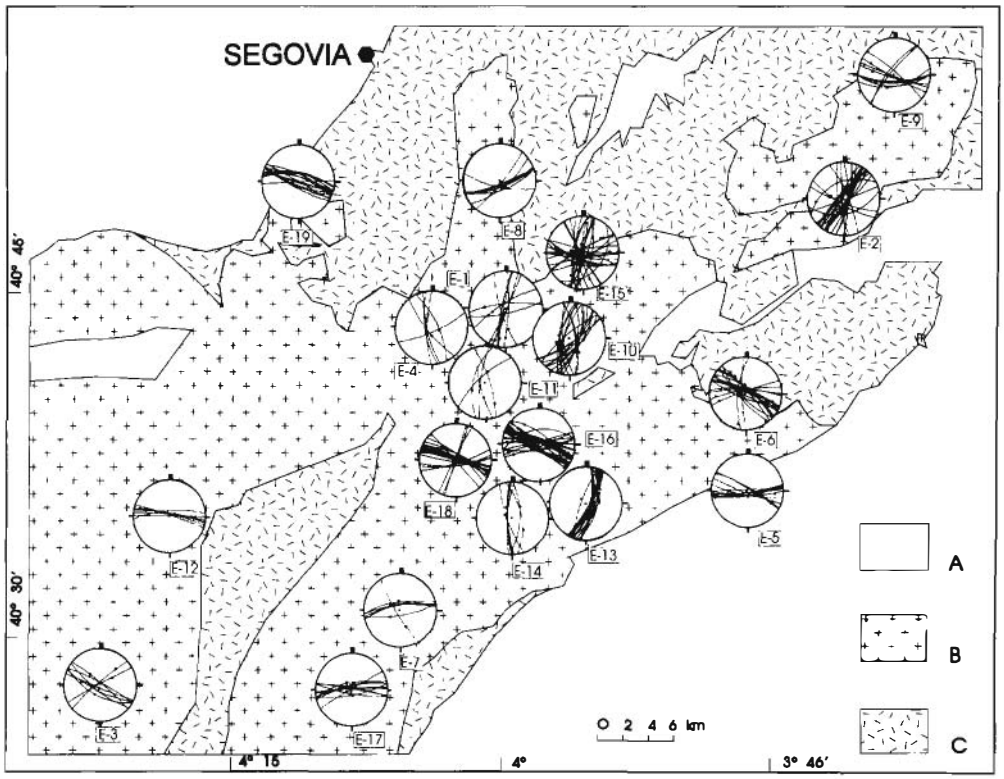


Fig. 4. Stereographic plots (Schmidt's projection, lower hemisphere) of faults and striae measured at several locations. *A* = post-Hercynian sediments; *B* = Hercynian granites; *C* = metamorphic rocks.

The magnitudes of the shear ($\tau$) and normal stresses ($\sigma_n$) satisfy the failure condition $\tau = \mu\sigma_n$ ($\mu$ = coefficient of friction), according to the Byerlee assumption ($\tau = 0.85\sigma_n$ when $3 < \sigma_n < 200$ MPa (Byerlee, 1978); (2) The slip event occurred under relatively uniform conditions. The calculation is made with values of the coefficient of friction ($\mu$) progressively increasing from 0 to 1, at intervals of 0.1. The output, for any value of $\mu$, consists of: (a) The orientation and magnitudes of $\sigma_1$, $\sigma_2$ and $\sigma_3$ relative to $\sigma_z = 100$; (b) The axial ratio [$\Phi = (\sigma_2 - \sigma_3)/(\sigma_1 - \sigma_3)$]; and (c) The misfit angle between the measured and the calculated striae. The selected solution is that which fits the largest number of faults with the minimum error, and has a coefficient of friction closer to 0.85, is the value corresponding to faults with $\sigma_n$ lower than 200 MPa (Byerlee, 1978). Those that do not fit the first solution probably formed under a different stress tensor. Thus, the method can be used to discriminate polyphase deformation.

– Third, at those places where the fault striations could not be measured (e.g., E-19, Fig. 4), the orientation of the principal stresses was inferred from the conjugate fault patterns by comparison with the theoretical faulting models of Anderson (1951) and Reches (1978, 1983).

## 5. Results

### *5.1. Fault versus episyenite orientations*

The rose diagram for the trends of the measured faults (Fig. 2B) shows that they can be grouped into three well-defined maxima: N80-90E (11%), N100-120E (20.5%) and N10-30E (18%). Dips are always

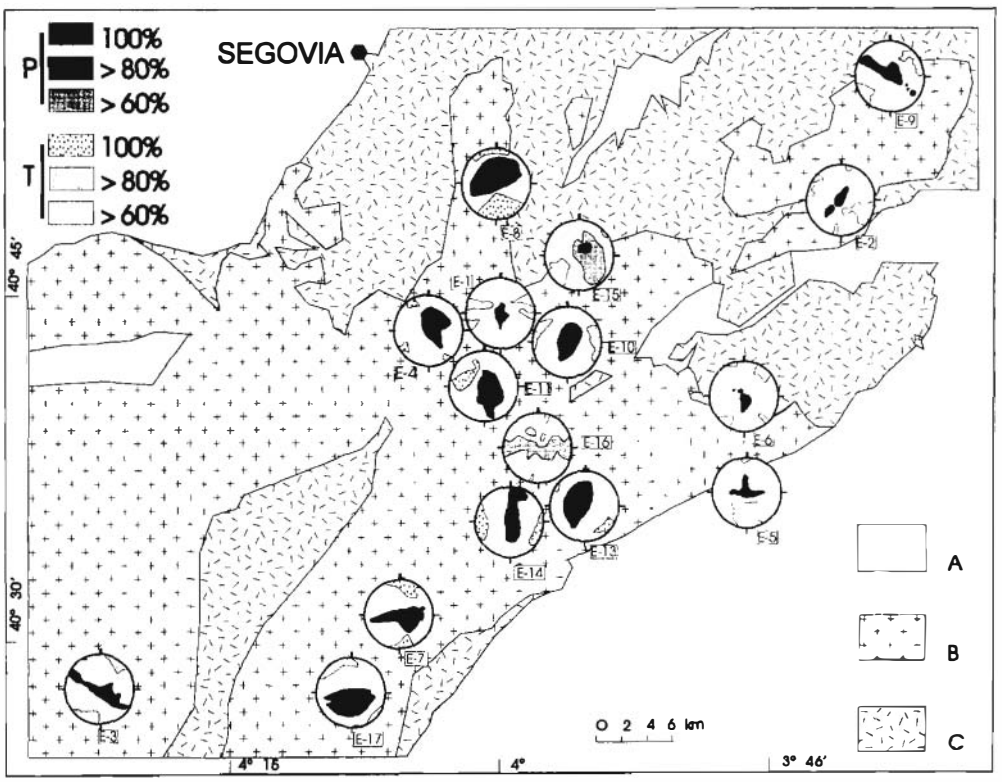


Fig. 5. Results of the striated-fault-plane analysis. Right-dihedra method (Angelier and Mechler, 1977). (*P*) compression areas and (*T*) tension areas on a stereographic projection (Schmidt's projection, lower hemisphere). Contours show the percentage of faults compatible with the domains of extension and compression. *A*, *B* and *C* as in Fig. 4.

high, 70% of the faults dipping more than 70°, both to the north and south (Figs. 2C and 4). Most of the faults show striations on the fault plane, with plunges of either 60–90° (47%) or 0–30° (33%) (Fig. 2D). The direction of movement is correspondingly normal dip-slip or normal oblique-slip. In all cases, faults show small offsets of some tens of centimeters. Fig. 4 shows the orientation of faults and striations at all the studied localities. In the central part of the area, fault trends are predominantly N–S, while in most other regions they are largely E–W.

At any locality, excepting E-15, most of the faults are arranged in a rhombic or orthorhombic symmetry, as expected from the models of Anderson (1951) and Reches (1983). In both cases, the episyenitic plane is commonly found to bisect the acute angle defined by the fault sets. This geometric coincidence provides a strong argument in favour of the formation of both faults and episyenites under the same stress field. In this respect, the case of E-15 is particularly relevant. Here, two orthogonal episyenitic bodies are found. Most of the faults can be grouped into two families, each formed by two sets, and each symmetrically arranged about the episyenitic planes in a manner similar to the other cases. At some localities faults exist that do not show a clear arrangement respective to the episyenite plane, e.g., at E-18 or E-4. These faults are probably younger.

### *5.2. Principal stress orientation and stress ratio*

The diagrams resulting from the application of the right-dihedra method for each location are shown in Fig. 5. The shortening axis (P) is consistently subvertical, with extension (T) consequently close to horizontal and oriented normal to the episyenitic bodies.

Results of the stress inversion method of Reches (1987) are summarized in Fig. 6 and Table 1. At

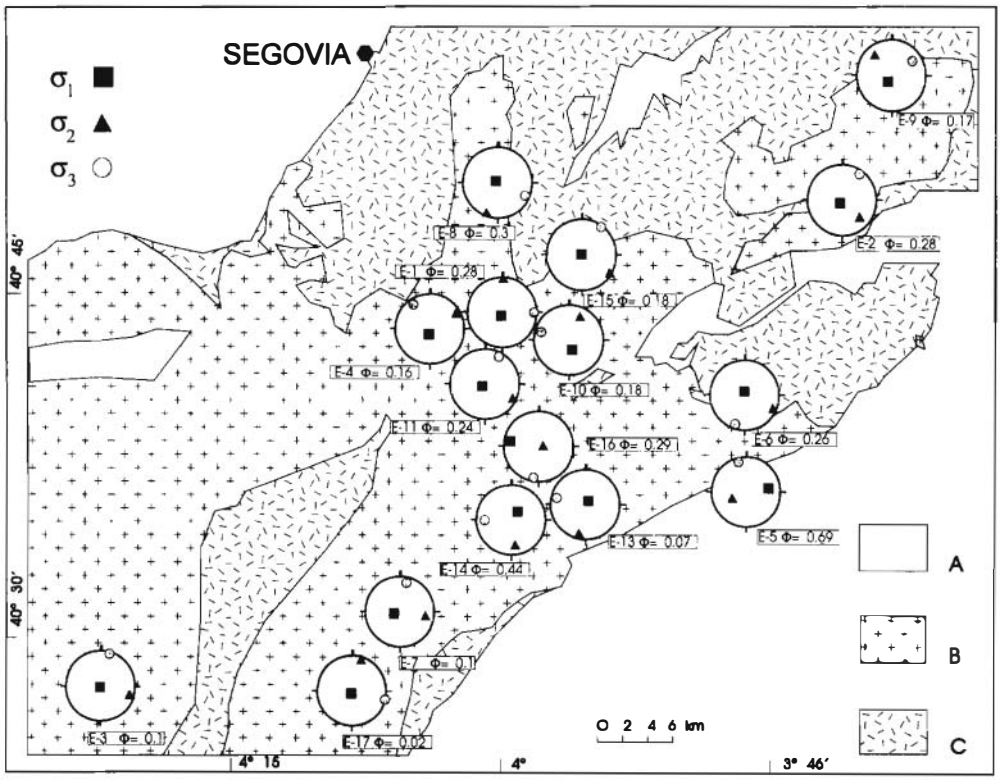


Fig. 6. Results of the striated fault plane analysis after the method of Reches (Reches, 1987). The symbols represent the orientation of the effective stresses on a stereographic plot [$\Phi = (\sigma_2 - \sigma_3)/(\sigma_1 - \sigma_3)$]. *A*, *B* and *C*, as in Fig. 4.

Table 1

Features of the stress tensor computed for each location (Reches method, 1987). $N$ is the number of faults defining the stress tensor, and $N_{t-t}$ is the total fault population. $T$ is the mean trend of the fault population. Dip and azimuth of the effective stress axes are in degrees. The $r_i$ value is the ratio of $i$th stress to the effective vertical load, values of the stresses relative to the vertical load (= 100). The stress ratio phi [$\Phi = (\sigma_2-\sigma_3)/(\sigma_1-\sigma_3)$] defines the shape of the stress ellipsoid. The $\mu$ represents the calculated coefficient of friction. The $\Delta$ is the average angle between striation and the orientation of theoretical maximum shear stress

| Station | $N(N_{t-t})$ | $T$ | $\sigma_1$ | $r_1$ | $\sigma_2$ | $r_2$ | $\sigma_3$ | $r_3$ | $\Phi$ | $\mu$ | $\Delta$(°) |
|---|---|---|---|---|---|---|---|---|---|---|---|
| E-1 | 8(10) | 22 | 79/194 | [102] | 10/0 | [41] | 2/90 | [17] | 0.28 | 0.5 | 31 |
| E-2 | 10(29) | 35 | 81/233 | [101] | 21/128 | [38] | 8/37 | [13] | 0.28 | 0.6 | 15 |
| | 9 | 45 | 80/218 | [102] | 5/341 | [21] | 7/72 | [11] | 0.11 | 0.8 | 30 |
| E-3 | 8(8) | 110 | 84/284 | [100] | 5/102 | [35] | 0/192 | [28] | 0.10 | 0.4 | 25 |
| E-4 | 6(6) | 162 | 81/186 | [102] | 5/56 | [22] | 6/326 | [6] | 0.16 | 0.8 | 10 |
| E-5 | 7(12) | 95 | 44/81 | [115] | 45/253 | [85] | 3/347 | [19] | 0.69 | 0.8 | 10 |
| E-6 | 10(20) | 120 | 80/354 | [102] | 5/116 | [45] | 8/206 | [17] | 0.26 | 0.7 | 7 |
| E-7 | 6(7) | 80 | 73/260 | [106] | 15/99 | [29] | 5/8 | [20] | 0.10 | 0.8 | 6 |
| E-8 | 8(8) | 70 | 86/319 | [100] | 1/207 | [25] | 3/116 | [23] | 0.30 | 0.7 | 8 |
| E-9 | 6(10) | 95 | 72/214 | [109] | 6/324 | [25] | 16/56 | [8] | 0.17 | 0.8 | 17 |
| E-10 | 14(20) | 22 | 68/164 | [110] | 18/18 | [37] | 11/284 | [20] | 0.18 | 0.8 | 10 |
| E-11 | 4(5) | 108 | 82/249 | [101] | 5/115 | [23] | 5/25 | [1] | 0.24 | 0.8 | 8 |
| E-12 | (7) | 100 | | | | | | | | | |
| E-13 | 10(15) | 20 | 81/36 | [101] | 7/186 | [26] | 4/276 | [20] | 0.07 | 0.8 | 11 |
| E-14 | 7(7) | 175 | 68/35 | [107] | 17/179 | [60] | 11/272 | [22] | 0.44 | 0.8 | 14 |
| E-15 | 17(30) | 208 | 89/130 | [100] | 0/305 | [38] | 0/35 | [25] | 0.18 | 0.4 | 31 |
| | 7 | 60 | 23/27 | [155] | 62/240 | [93] | 13/123 | [38] | 0.46 | 0.5 | 21 |
| E-16 | 16(27) | 105 | 10/281 | [226] | 79/86 | [96] | 2/190 | [42] | 0.29 | 0.8 | 19 |
| | 9 | 115 | 78/129 | [100] | 4/18 | [99] | 10/287 | [96] | 0.81 | 0.0 | 22 |
| E-17 | 10(10) | 85 | 86/205 | [100] | 3/15 | [16] | 0/105 | [14] | 0.02 | 0.8 | 8 |
| E-18 | (19) | 110 | | | | | | | | | |
| E-19 | (17) | 109 | | | | | | | | | |

most localities the percentage of faults that the tensor solution fits is close to 100 (e.g., E-1, E-3, E-4, E-7, E-8,...). In these cases the computed location of $\sigma_1$ is close to vertical, the only exception being E-5, where $\sigma_1$ is subhorizontal. At three locations (E-2, E-15 and E-16), more than one tensor fits the measured fault population; in two of them (E-15 and E-16), one of the solutions shows $\sigma_1$ subvertical, whilst in the second $\sigma_1$ is subhorizontal. In fact, part of the measured planes at these locations show low-plunging striae (Fig. 4). Field evidence, i.e., cross-cutting relationships, suggests that the latter faults are younger than those with high-plunging striae. However, considering the aforementioned rhombic symmetry of the faults, we interpret that at these locations (and probably E-5 too) some of the former normal faults were reactivated as strike-slip faults during a deformation event younger than episyenites.

All the tensors having $\sigma_1$ subvertical show $\sigma_2$ and $\sigma_3$ axis oriented E–W and NNE–SSW respectively, $\sigma_3$ usually being close to normal to the episyenitic bodies. The main parameters relative to these tensors are: coefficient of friction between 0.4 and 0.8 (mean 0.71), and a stress ratio between 0.02 and 0.69.

### 5.3. *Principal stress magnitude*

The absolute values of the principal stresses have been left unknown in the numerical procedures outlined above. However, their magnitudes can be estimated in several ways (e.g., Bergerat et al., 1985; Angelier, 1989; Gil-Peña and Simón-Gómez, 1992). Currently, the first step is an estimate of the palaeodepth during the faulting episode and, consequently, the lithostatic pressure. Depending on the tectonic regime, this value must be close to either $S_1$, $S_2$ or $S_3$ ($S_i$ = principal stresses). Assuming dry conditions, this value must also be similar to the effective stress $\sigma_1$, $\sigma_2$ or $\sigma_3$ ($\sigma_i = S_i - P_1$, assuming Terza-

Table 2
Value of the principal stresses ($S_1$, $S_2$ and $S_3$) scaled with respect to the estimated vertical load. Locations with extensional stress tensors have only been considered. Hydrostatic conditions for the fluid pressure are assumed (see text for explanation)

| Station | $S_1$ Min (MPa) | $S_2$ Min (MPa) | $S_3$ Min (MPa) |
|---|---|---|---|
| E-1 | 172 | 108 | 83 |
| E-2 | 171 | 105 | 79 |
| E-3 | 170 | 102 | 94 |
| E-4 | 172 | 88 | 71 |
| E-5 | - | - | - |
| E-6 | 172 | 112 | 83 |
| E-7 | 179 | 95 | 86 |
| E-8 | 170 | 91 | 89 |
| E-9 | 179 | 91 | 73 |
| E-10 | 181 | 104 | 86 |
| E-11 | 171 | 89 | 66 |
| E-12 | - | | |
| E-13 | 171 | 92 | 86 |
| E-14 | 177 | 128 | 88 |
| E-15 | 170 | 104 | 91 |
| E-16 | - | - | - |
| E-17 | 170 | 82 | 80 |
| E-18 | - | - | - |
| E-19 | - | - | - |
| Mean | 173 | 99 | 82 |
| Standard deviation | 3 | 11 | 7 |

ghi's law). As the faulting episode was extensional it follows that the lithostatic pressure had to be close to $S_1$ (6.5 km ≅ 170 MPa). Now, assuming that the rocks were water saturated, and that $P_f$ was equivalent to the hydrostatic head ($P_f$ = 65 MPa, i.e., ≈ 10 MPa km$^{-1}$), the magnitude of the effective stresses relative to the effective vertical load calculated for each locality (values within brackets in Table 1) can be converted into absolute values of the principal stresses (Table 2) by taking into account that:

$$\sigma_i = r_i \sigma_v = r_i (S_v - P_f)$$

and

$$S_i = \sigma_i + P_f$$

where $\sigma_v$ and $S_v$ are the effective vertical load and the vertical principal stress respectively, and $r_i$ is the ratio of $i$th stress to the effective vertical load. Average values of the principal stresses obtained in this way are: $S_1$ = 173 MPa, $S_2$ = 99 MPa and $S_3$ = 82 MPa. A note of caution is that these values of $S_2$ and $S_3$ are minimum values as $P_f$ was probably larger than the hydrostatic head, particularly at the onset of every pulse of fracturing.

### 5.4. *Palaeostress field*

Based on the above conclusions, particularly that the location of $\sigma_3$, as resulting from fault population analysis, is subhorizontal and normal to the episyenitic bodies, both fault analysis and orientation of episyenites themselves can be used to map $\sigma_3$ trajectories over the studied area. However, a problem is posed in the central part of the Sierra del Guadarrama, where two orthogonal sets of faults and episyenite orientations, are often found at the same locality (Fig. 4). This fact, along with the low values of phi, suggests that extension was bidirectional in many places. It is remarkable that this region also presents other significant N–S features that are clearly older, such as an elongated monzogranite pluton which occupies the core of a Hercynian fold, and a dyke swarm of few – but very long – granite porphyries and some microdiorites (Fig. 1). This strongly suggests that this domain is an old weakness zone, N–S episyenites thus probably resulting from its reactivation in the form of extension parallel to the regional $\sigma_2$ axis. The $\sigma_3$ axis obtained from these episyenites is therefore disregarded.

The transformation of local scattered directional data into a map of $\sigma_3$ trajectories was carried out, using the distance-weighting method proposed by Lee and Angelier (1994), which is based on an inverse distance weighting function, the degree of smoothness of trajectories being controlled by the power value and threshold distance (Fig. 7B). In this computation the episyenites with a $\sigma_3$ axis close to E–W and the fault solutions with subhorizontal $\sigma_1$ axis have not been considered.

## 6. Geotectonic interpretation

Structural analysis of faults related to the episyenitic bodies strongly suggests that at approx. 277 Ma the Spanish Central System underwent regional extension, with a main NNE–SSW extension direction. We also infer that this extensional episode was accompanied by a regional thermal anomaly characterized by widespread episyenite formation due

to fluid/rock interactions at temperatures between 350°C and 650°C.

The precise dating of this extensional tectonothermal episode, along with other new geochronological evidence, allows us to constrain the geotectonic evolution of the eastern Iberian Central System be-

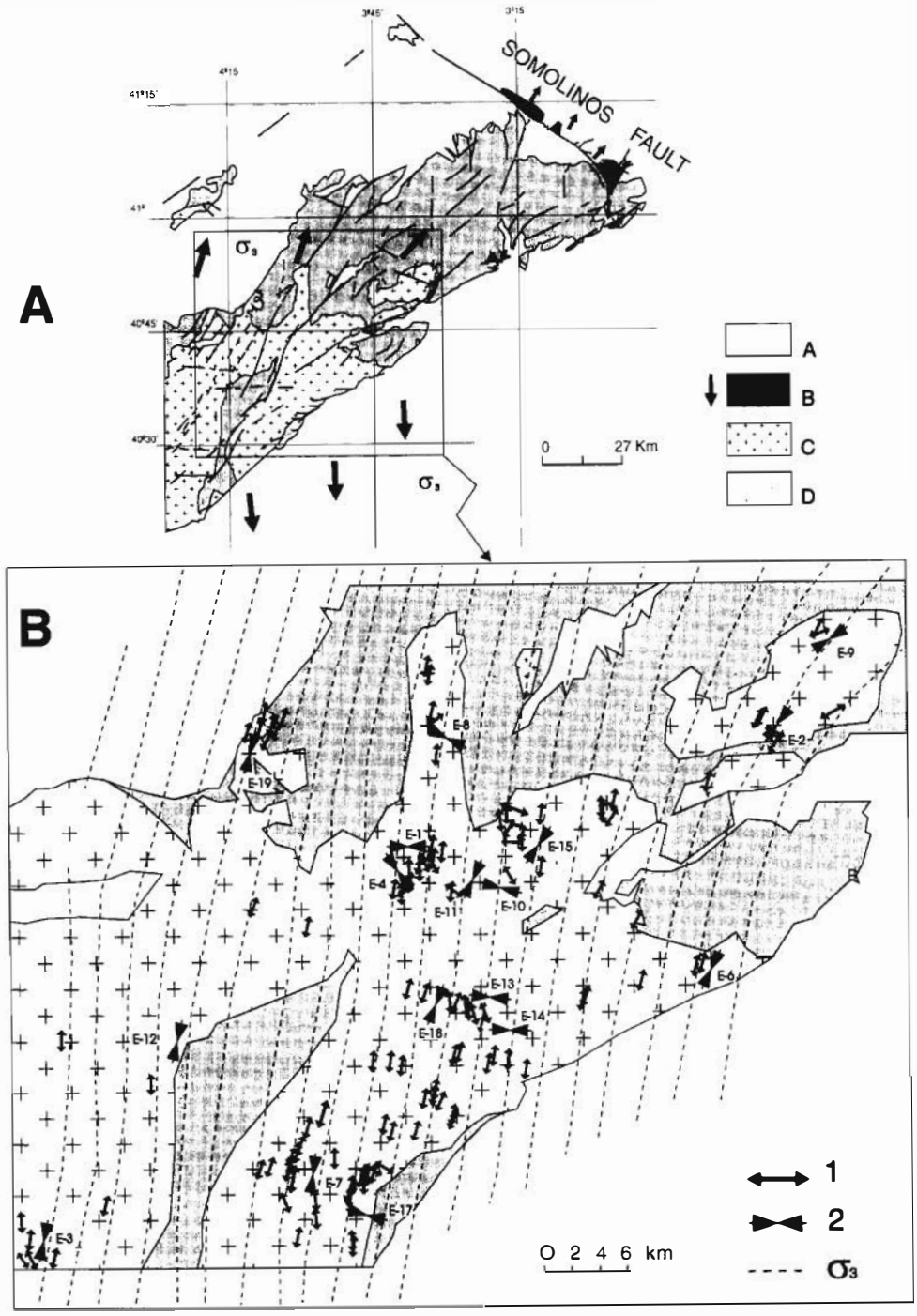

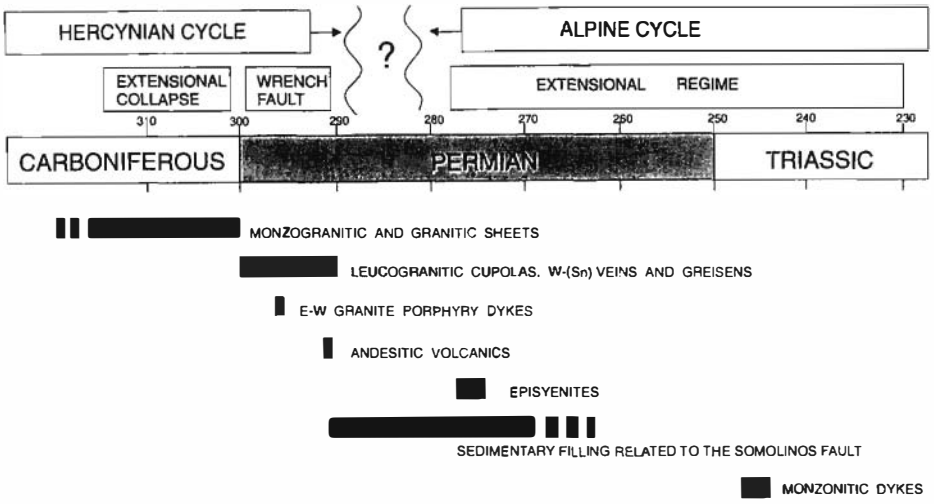


Fig. 8. Schematic diagram showing the geotectonic evolution of the studied region and the main chronostratigraphical features.

tween the Late Carboniferous and the Triassic (Fig. 8). The history of this period can be divided into three stages: a first, corresponding to the extensional collapse of the thickened Hercynian orogenic belt; a second, equivalent to the Late Variscan event of Arthaud and Matte (1977), during which the Iberian peninsula was part of a right-lateral megashear zone separating the Africa and Europe plates, and deformation inside Iberia was accommodated through a complex network of conjugate wrench faults and a third stage corresponding to a generalized distensive regime, which is unanimously assigned to the Alpine Cycle (Alvaro et al., 1979; Vegas and Banda, 1982; Casquet et al., 1988; Sopeña et al., 1988; González-Casado et al., 1993; Doblas et al., 1994).

However, some of these evolutionary models rely on quite scanty chronological information and stratigraphic evidence, which is particularly true for the Late Carboniferous and the Permian. Consequently, the precise time boundaries of the three stages, and the timing of many geological processes, particularly the igneous and hydrothermal ones, may be somewhat speculative.

The wrench-faulting stage can now be located more precisely in the time span 290–300 Ma, i.e., Late Carboniferous, on the basis of ages of W–(Sn) quartz veins and greisens that are clearly controlled by this compressional stress-field (González-Casado et al., 1993; Quílez, 1994) (Fig. 8). In this period, the horizontal shortening direction in this part of the Iberian plate was orientated N100-130E, depending on location (Quílez, 1994). A similar orientation has also been suggested for part of the wrench-faulting episode by Ziegler (1990).

Within the error of the geochronological data, E–W dyke injection in the Sierra del Guadarrama also took place – at least in part – during the same period ($296 \pm 3$ Ma; Galindo et al., 1994b). The

Fig. 7. (A) Geological sketch of the Sierra del Guadarrama, and its eastward continuation into the Iberian Range, during the extensional tectono-thermal episode leading to episyenite formation ($\approx 277$ Ma). Large arrows represent the inferred direction of extension in the surveyed area. Small arrows are transport direction of sediments during the extensional movement of the Somolinos fault (Pérez-Mazario et al., 1992), which is here correlated with episyenite formation in the basement. *A* = post-Hercynian sediments; *B* = Permian sediments; *C* = Hercynian granites; *D* = metamorphic rocks. (B) Trajectories of $\sigma_3$ in the studied area, obtained by applying the distance-weighting method of Lee and Angelier (1994) to the local trend of $\sigma_3$ deduced from fault analysis (*2*) and episyenite orientations (*1*). In this computation, episyenites with a $\sigma_3$ axis close to E–W and tensor with axes $\sigma_1$ subhorizontal have not been considered.

exact field stress during dyke emplacement is still unclear; however, a clear genetic relationship can be found between high level dykes and small granitic cupolas and W–(Sn–Mo) quartz veins and greisens (Tornos et al., 1993). Therefore, it is reasonable to suggest that dyke injection probably took place as part of this same wrench-faulting episode, as already suggested by González-Ubanell and Doblas (1987) and Casquet et al. (1988).

The Somolinos fault, which is a major NW–SE-trending fault located at the SCS–Iberian Range boundary (Fig. 7A), had a left-lateral strike-slip motion, controlling the filling of small transtensional intermontane detrital sedimentary basins (Pérez-Mazario et al., 1992). The effusion of andesitic lavas and volcanoclastic material also took place along the Somolinos fault in this stage, as suggested by the spatial relationship between fault and vulcanites, and the recalculated age of the andesites from Atienza [291 ± 12 Ma; age corrected with the Steiger and Jaeger (1977) constant, after a K–Ar apparent age given by Hernando et al. (1980)].

The period between 290 and 277 Ma has still not been recorded radiometrically, and therefore the interpretation is quite conjectural, although sedimentation in the intermontane basins probably persisted for some time, the Somolinos fault inverting in this period to a right-lateral motion (Pérez-Mazario et al., 1992). Ages provided by the episyenites suggest that generalized extensional conditions prevailed at about 277 Ma, i.e., Early Permian. This is here taken as the onset of the Alpine Cycle. The new extensional situation led to movements of the Somolinos fault – and others – with an important vertical component, which controlled the deposition of the Lower Permian (Autunian) upper sedimentary units (Pérez-Mazario et al., 1992). This behavior of the Somolinos fault is in fact to be expected under the stress-field deduced for the episyenites, and the two are therefore tentatively correlated here.

We suggest that Saxonian-type red sediments that lay unconformably over the Autunian rocks were probably deposited under generalized extensional conditions that persisted to – at least – the Late Permian–Early Triassic boundary. This is suggested by the existence of the alkaline dykes in the Sierra del Guadarrama dated at 245 ± 7 Ma (Galindo et al., 1994b).

## 7. Conclusions

Episyenitization of granitic rocks in the Sierra del Guadarrama took place at about 277 Ma, at an estimated depth of about 6.5 km, through the action of low salinity aqueous fluids at temperatures of 350 to 600°C. These fluids percolated through a dense set of lens-shaped microfracturated domains, which represent dilatancy volumes developed parallel to the maximum principal stress, i.e., $S_1$. Formation of discrete faults eventually took place inside these volumes. The analysis of the striated faults, using several computer-aided methods, along with the statistical analysis of the orientation of the episyenitic bodies, shows that the episyenites and their related faults resulted from an extensional stress regime (with a stress ratio between 0.02 and 0.69, and principal stresses of $S_1$ close to 173 MPa and minimum values of $S_2$ and $S_3$ of 99 and 82 MPa respectively) and a horizontal principal extension axis oriented NNE–SSW. Older N–S structural anisotropies present in the central part of the study area probably controlled the orientation of some episyenites there.

Episyenites also indicate that a regional thermal anomaly existed in the area during the extensional episode, as evidenced by the moderate to high temperatures of fluids involved in the process. Episyenites from the Sierra del Guadarrama can thus be considered as representatives of dewatering of the crust under an extensional tectono-thermal regime.

The tectono-thermal event represented by the episyenites followed an episode of generalized wrench faulting, during which an acid hydrothermal alteration (Sn–W), the emplacement of evolved peraluminous leucogranites, dyke injection and local effusion of andesites took place. This event has been dated at 290–300 Ma, and corresponds to the so-called Late Variscan event of Arthaud and Matte (1977). The tectono-thermal event leading to the episyenite formation can thus be taken as being representative of the beginning of the Alpine Cycle in central Iberia.

## Acknowledgements

Financial support for this work was provided by the Spanish Government D.G.I.C.Y.T. grant PB 88-

0124. Thanks are also due to Alfonso Muñoz and Dr. Gerardo de Vicente for their version of fault slip analysis programs, and to Dr. Jiang-Cheng Lee for his computer program for calculating stress trajectory maps (Lissage routine). We thank E. Barrier and an anonymous referee for constructive reviews that helped us to improve the quality of the manuscript.

## References

Alvaro, M., Capote, R. and Vegas, R., 1979. Un modelo de evolución geotectónica para la cadena Celtibérica. Acta Geol. Hisp., 14: 172–177.

Anderson, E.M., 1951. The Dynamics of Faulting. Oliver and Boyd, Edinburgh, 206 pp.

Angelier, J., 1979. Determination of the mean principal stresses for a given fault population. Tectonophysics, 56: T17–T26.

Angelier, J., 1989. From orientation to magnitudes in paleostress determinations using fault slip data. J. Struct. Geol., 11: 37–50.

Angelier, J. and Mechler, P., 1977. Sur une méthode graphique de recherche des constraintes principales également utilisable en tectonique et en séismologie: le méthode des dièdres droits. Bull. Soc. Géol. Fr., 7: 1309–1318.

Arthaud, F. and Matte, F., 1977. Late Palaeozoic strike-slip faulting in southern Europe and northern Africa: Result of a right-lateral shear zone between the Appalachians and the Urals. Geol. Soc. Am. Bull., 88: 1305–1320.

Atkinson, B.K., 1984. Subcritical crack growth in geological materials. J. Geophys. Res., 89: 4077–4114.

Bergerat, F., Berges, J. and Geyssant, J., 1985. Estimation des paléo-cointrantes liées a la formation de décrochements dans la plate-forme d'Europe du Nord. Geol. Rundsch., 74: 311–320.

Bott, M.H.P., 1959. The mechanics of oblique slip faulting. Geol. Mag., 96: 109–117.

Byerlee, J.D., 1978. Friction of rocks. Pure Appl. Geophys., 116: 615–626.

Caballero, J.M., 1993. Las Episienitas de la Sierra de Guadarrama: Un Caso Singular de Alteración Hidrotermal de Edad Post-hercínica. Thesis, Univ. Complutense Madrid, 313 pp.

Caballero, J.M., Casquet, C., Tornos, F. and Pellicer, M.J., 1991. Caracterización petrográfica de las episienitas de la Sierra del Guadarrama, Sistema Central Español S.C.E. Bol. Soc. Esp. Min., 14: 273–284.

Caballero, J.M., Casquet, C., Galindo, C., González Casado, J.M., Snelling, N. and Tornos, F., 1992. Dating of hydrothermal events in the Sierra del Guadarrama, Iberian Hercynian Belt, Spain. Geogaceta, 11: 18–22.

Caballero, J.M., Casquet, C., Galindo, C., González Casado, J.M., Pankhurst, R. and Tornos, F., 1993. Geocronología por el método Rb–Sr de las episienitas de la Sierra del Guadarrama, S.C.E. Geogaceta, 13: 16–18.

Capote, R., González-Casado, J.M. and De Vicente, G., 1987. Análisis poblacional de la fracturación tardihercínica en el sector central del Sistema Central Ibérico. Cuad. Lab. Xeol. Laxe, 11: 305–311.

Carey, E. and Brunier, B., 1974. Analyse théorique et númerique d'un modele mécanique élémentaire appliqué á l'etude d'une population de failles. C.R. Acad. Sci. Paris, 179: 891–894.

Casas Sainz, A.M., Gil Peña, I. and Simón Gómez, J.L., 1988. Los métodos de análisis de paleoesfuerzos a partir de poblaciones de fallas: sistemática y técnicas de aplicación. Estud. Geol., 46: 385–398.

Casillas, R., Vialette, Y., Peinado, M., Duthou, J.L. and Pin, C., 1991. Ages et caracteristiques isotopiques Sr–Nd des granitoides de la Sierra de Guadarrama Occidentale Espagne. In: R. Black, B. Bonim, A. Giret and P. Sabate (Editors), Granites Oceaniques et Continentaux. Seance specialisée de la Societé Geologique de France, Paris.

Casquet, C., Fúster, J.M., González Casado, J.M., Peinado, M. and Villaseca, C., 1988. Extensional tectonics and granite emplacement in the Spanish Central System. A discussion. In: E. Banda and L.A. Mendes-Victor (Editors), Fifth EGT Workshop: The Iberian Peninsula, pp. 65–77.

Casquet, C., Caballero, J.M., Galindo, C. and Tornos, F., 1992. A revised model for the formation of dequartzified and alkalinized granites episyenites. In: Y. Kharake and A. Maest (Editors), Water–Rock Interaction, 2. Balkema, Rotterdam, pp. 1481–1484.

Cathelineau, M., 1985. Episyenitization ou dequartizitification hydrothermale: une typologie basée sur les successions mineralogiques et sur le component diferential de Si, Na, et K. C.R. Acad. Sci. Paris, 300(Ser. II 14): 677–680.

Crampin, S., 1987. Geological and industrial implications of extensive-dilatancy anisotropy. Nature, 328: 491–496.

De Vicente, G., González-Casado, J.M., Bergamin, J.F., Tejero, R., Babín, R., Rivas, A., Hernández-Henrile, J.L., Giner, J., Sánchez-Serrano, F., Muñoz, A. and Villamor, P., 1992. Alpine structure of the Spanish Central System. In: Actas III Congr. Geol. España, Tomo 1: 284–288.

De Vicente, G., Muñoz, A. and Giner, J., 1992b. El uso práctico del método de los diedros rectos: implicaciones desde el modelo de deslizamiento del análisis poblaciones de fallas. Rev. Soc. Geol. Esp., 5: 7–19.

De Vicente, G., González-Casado, J.M., Giner, J., Muñoz-Martín, A. and Rodríguez-Pascua, M.A., 1996. Structure and alpine evolution of the Madrid Basin. In: P. Friend and C. Dabrio (Editors), Tertiary Basins of Spain. Cambridge University Press, pp. 263–267.

Doblas, M., Oyarzun, R., Sopeña, A., López Ruiz, J., Capote, R., Hernández Enrile, J.L., Hoyos, M., Lunar, R. and Sánchez Moya, Y., 1994. Hercynian–late Hercynian–early Alpine progressive extensional collapse of Central Spain. Geod. Acta, 7: 1–14.

Etchecopar, A. and Mattauer, M., 1988. Méthodes dynamiques d'analyse des populations de failles. Bull. Soc. Géol. Fr., 8: 289–302.

Etchecopar, A., Vasseur, G. and Daignières, M., 1981. An inverse

problem in microtectonics for the determination of stress tensors from fault striation analysis. J. Struct. Geol., 3: 51–65.

Galindo, C., Tornos, F., Darbyshire, and Casquet, C., 1994. The age and origin of the barite–fluorite (Pb–Zn) veins of the Sierra del Guadarrama (Spanish Central System, Spain): a radiogenic (Nd, Sr) and stable isotope study. Chem. Geol., 112: 351–364.

Galindo, C., Huertas, M.J. and Casquet, C., 1994b. Rb–Sr and K–Ar chronology of dykes from the Sierra de Guadarrama Spanish Central System. Geogaceta, 16: 23–26.

Gebauer, D., Martinez-García, E. and Hepburn, J.C., 1993. Geodinamic significance, age and origin of the Ollo de Sapo Augengneiss, NW Iberian Massif, Spain. In: Geol. Soc. Am. Annu. Meet., abstract A-342.

Gil-Peña, I. and Simón-Gómez, J.L., 1992. Aproximación al cálculo de los valores absolutos de paleoesfuerzos compresivos en el Mioceno Inferior de Tudela (Navarra). Geogaceta, 11: 31–34.

González-Casado, J.M., Casquet, C., Caballero, J.M., Galindo, C., Quílez, E. and Tornos, F., 1993. Análisis de la fracturación asociada a las alteraciones hidrotermales de tipo Greisen y Episienita en la Sierra de Guadarrama. Geogaceta, 13: 56–59.

González-Uhanell, A. and Doblas, M., 1987. Los diques aplíticos deformados de Paredes de Escalona–Navamorcuende (SW del Sistema Central Español): Su relación con la intrusión. In: F. Bea, A. Carnicero, J.C. Gonzalo, M. López Plaza and M.D. Rodríguez Alonso (Editors), Geología de los Granitoides y Rocas Asociadas del Macizo Hespérico. Rueda, Madrid, pp. 393–403.

Holcomb, D.J. and Stevens, J.L., 1980. The reversible Griffith crack: A viable model for dilatancy. J. Geophys. Res., 85: 7101–7107.

Hernando, S., Schott, J.J., Thuizat, R. and Montigny, R., 1980. Ages des andésites et des sédimentes interstratifiés de la région d'Atienza Espagne: étude stratigraphique, géochrolologique et paléomagnétique. Soc. Geol. Bull., 33: 119–128.

Huertas, M.J., 1991. Las Asociaciones Filonianas Tardihercínicas en la Sierra de Guadarrama S.C.E. Thesis, Univ. Complutense Madrid, 335 pp.

Ibarrola, E., Villaseca, C., Vialette, Y., Fúster, J.M., Navidad, M., Peinado, M. and Casquet, C., 1987. Dating of hercynian granites in the Sierra de Guadarrama Spanish Central System. In: F. Bea, A. Carnicero, J.C. Gonzalo, M. López Plaza and M.D. Rodríguez Alonso (Editors), Geología de los Granitoides y Rocas Asociadas del Macizo Hespérico. Rueda, Madrid, pp. 377–384.

Lee, J.-Ch. and Angelier, J., 1994. Paleostress trajectory maps based on the results of local determinations: the "Lissage" program. Comput. Geosci., 20: 161–191.

Leroy, J., 1982. Le gissement du Bernandan. Etude mineralogiques, chimiques et des inclusions fluides de l'episyénitisation. In: Rapport CREGU Nº82-1, 93 pp.

Lespinasse, M., 1984. Contexte structural des gisements d'uranium de la Marche Occidentale fracturation, circulations fluides, propagation de l'épisyenitisation. Géologie et Géochimie de l'Uranium, 8, 196 pp.

Lisle, R.J., 1987. Principal stress orientations from faults: an additional constraint. Ann. Tectonicae, 1: 155–158.

Lockner, D.A., Byerlee, J.D., Kuksenko, V., Ponomared, A. and Sidorin, A., 1991. Quasi-static fault growth and shear fracture energy in granite. Nature, 350: 39–42.

Lovell, J.H., Crampin, S. and Shepherd, T.J., 1990. Stress in the Earth's crust: the link between crustal fluids and extensive-dilatancy anisotropy. J. Geol. Soc. London, 147: 971–978.

Michael, A.J., 1984. Determination of stress from slip data: faults and folds. J. Geophys. Res., 89: 11,517–11,526.

Pecher, A., Lespinasse, M. and Leroy, J., 1985. Relations between fluid inclusion trails and regional stress field: a tool for fluid chronology—An example of an intragranitic uranium ore deposit northwest Massif Central, France. Lithos, 18: 229–237.

Pérez-Mazario, F., Hernando, S. and Rincón, R., 1992. Evolución en dos etapas de las cuencas pérmicas del borte noreste del Sistema Central Español. Análisis sedimentológico y procedencia de materiales. Cuad. Geol. Ibérica, 16: 91–114.

Pérez-Soba, C., 1991. Petrología y Geoquímica del Macizo Granítico de la Pedriza, Sistema Central Español. Thesis, Univ. Complutense Madrid, 225 pp.

Quílez, E., 1994. Mineralizaciones Filonianas de Wolframio de la Sierra de Guadarrama: Modelo y Caracterización del Proceso Hidrotermal. Thesis, Univ. Complutense Madrid, 277 pp.

Reches, Z., 1978. Analysis of faulting in three-dimensional strain field. Tectonophysics, 47: 109–129.

Reches, Z., 1983. Faulting of rocks in three-dimensional strain field. II. A strain theory of faulting. Tectonophysics, 95: 133–156.

Reches, Z., 1987. Determination of the tectonic stress tensor from slip along faults that obey the Coulomb Yield condition. Tectonics, 6: 849–861.

Reches, Z., Baer, G. and Hatzor, Y., 1992. Constraints on the strength of the upper crust from stress inversion of fault slip data. J. Geophys. Res., 97: 12,481–12,493.

Rutter, E.H., 1986. On the nomenclature of mode of failure transitions in rocks. Tectonophysics, 122: 381–387.

Salas, R. and Casas, A., 1993. Mesozoic extensional tectonics, and crustal evolution during the alpine cycle of the eastern Iberian basin. Tectonophysics, 228: 33–55.

Simón Gómez, J.L., 1986. Analysis of a gradual change in stress regime example from eastern Iberian Chain, Spain. Tectonophysics, 124: 37–53.

Sopeña, A., López, J., Arche, A., Pérez Arlucea, M., Ramos, A, Virgili, C. and Hernando, S., 1988. Permian and Triassic Rift-Basins of the Iberian Peninsula. In: W. Manspiezer (Editor), Triassic–Jurassic Rifting. Dev. Geotectonics, 22: 757–786.

Steiger, R.H. and Jaeger, E., 1977. Subcomission on geochronology: Convection on the use of decay constant in geo and cosmochronology. Earth Planet. Sci. Lett., 36: 359–362.

Tornos, F., 1989. Los Skarns y Mineralizaciones Asociadas del Sistema Central Español. Thesis, Univ. Complutense Madrid. 497 pp.

Tornos, F., Casquet, C. and Caballero, J.M., 1993. La alteración hidrotermal asociada al plutón epizonal de Navalcubilla, Sierra del Guadarrama (Sistema Central Español). Rev. Soc. Geol. España, 6: 67–83.

Vegas, R. and Banda, E., 1982. Tectonic framework and alpine evolution of the Iberian Peninsula. Earth Evol. Sci., 4: 320–343.

Vialette, Y., Bellido, F., Fúster, J.M. and Ibarrola, E., 1981. Données géochronologiques sur les granites de La Cabrera. Cuad. Geol. Ibérica, 7: 327–335.

Vialette, Y., Casquet, C., Fúster, J.M., Ibarrola, E., Navidad, M., Peinado, M. and Villaseca, C., 1987. Geochronological study of orthogneisses from the Sierra de Guadarrama S.C.S. Neues Jahrb. Mineral. Monatsh., 10: 465–479.

Wallace, R.E., 1951. Geometry of shearing stress and relation to faulting. J. Geol., Chicago, 59: 118–130.

Yanagidani, T., Ehara, S., Nishizawa, O. and Kusunose, K., 1985. Localization of Dilatancy in Oshima Granite Under Constant Uniaxial Stress. J. Geophys. Res., 90: 6840–6858.

Yukutake, H., 1989. Fracturing process of granite inferred from measurements of spatial and temporal variations in velocity during triaxial deformations. J. Geophys. Res., 11: 15,639–15,651.

Zhixin, X. and Walther, J.V., 1993. Quartz solubilities in NaCl solutions with and without wollastonite at elevated temperatures and pressures. Geochim. Cosmochim. Acta, 57: 1947–1955.

Ziegler, P.A., 1990. Geological Atlas of Western and Central Europe. Geol. Soc. London, 238 pp.